

Brown, Louise P. and Zeng, Xuesen and Long, Andrew C. and Brooks, Richard and Jones, I. Arthur (2013) Predicting the coefficient of thermal expansion for textile composites based on a unit cell approach. In: Texcomp-11 Conference, 16-20 September 2013, Leuven, Belgium.

Access from the University of Nottingham repository:

http://eprints.nottingham.ac.uk/3268/1/Predicting_the_CTE_for_textile_composites_based_on_a_unit_cell_approach.pdf

Copyright and reuse:

The Nottingham ePrints service makes this work by researchers of the University of Nottingham available open access under the following conditions.

This article is made available under the University of Nottingham End User licence and may be reused according to the conditions of the licence. For more details see:
http://eprints.nottingham.ac.uk/end_user_agreement.pdf

A note on versions:

The version presented here may differ from the published version or from the version of record. If you wish to cite this item you are advised to consult the publisher's version. Please see the repository url above for details on accessing the published version and note that access may require a subscription.

For more information, please contact eprints@nottingham.ac.uk

PREDICTING THE COEFFICIENT OF THERMAL EXPANSION FOR TEXTILE COMPOSITES BASED ON A UNIT CELL APPROACH

Louise P. Brown, Xuesen Zeng*, Andrew C. Long, Richard Brooks, I. Arthur Jones

Faculty of Engineering – Division of Materials, Mechanics & Structures, University of Nottingham, University Park, Nottingham, NG7 2RD, U.K.

*corresponding author: xuesen.zeng@nottingham.ac.uk

ABSTRACT The study focuses on unit cell FE modelling to predict coefficients of thermal expansion (CTEs) for sheared fabric laminates. Shear, as a dominant deformation mode in textile composites forming, introduces high degrees of anisotropy in both elasticity and thermal expansion. The unit cell predictions are based on realistic fibre architecture and measured material properties of constituent fibre and resin. Under the multi-scale framework, the unit cell predictions are part of the essential input data for locally varied material definitions. These definitions are used to model structural components to predict shape distortion. The FE model gives predictions close to the experimental data, when the boundary conditions are correlated to the coupon size. Nesting is an influential factor for CTEs. For true material representation, in-plane periodicity and nesting have been considered.

INTRODUCTION

Shape distortion of composite components is a common problem in composites manufacturing. The major cause of shape distortion is anisotropic thermal expansion, which would impact not only on the manufacturing process but also the in-service performance [1]. There is a large body of work dedicated to quantifying the coefficient of thermal expansion for fibre reinforced composites analytically. A critical review [2] on analytical models for UD composites reveals that only Hashin's model consistently predicts well both longitudinal and transverse CTEs. To overcome the cumbersome calculation process of Hashin's model, Dong's model was derived based on finite element analysis, facilitating accurate prediction of transverse CTE by a single equation [3]. For cross-ply and woven composites, a number of analytical models are available [4-6], however their accuracy suffers as over-simplifications are made regarding local fibre architectures. Due to the increasing thermal anisotropy for textile composites, experimental techniques such as thermoelastic stress analysis prove to be questionable to quantify the fully anisotropic CTE tensor [7].

Finite element unit cell modelling remains the most promising approach for predicting the CTE tensor with the advantages of consistency and cost saving. A unit cell model was developed for predicting CTEs of 4-ply twill fabric laminate composites [8]. There was a large difference (100% error) between the prediction and the experimental data. One possible source of error could have arisen from accuracy of the geometric model.

The current study focuses on the geometric aspects of unit cell modelling for CTE predictions. It aims to improve the quality of prediction, i.e. accuracy, consistency and efficiency by automated creation of realistic geometries in TexGen¹. The geometric description of a sheared fabric (representing deformation during draping) considers yarn rotations as two elliptical cylinders crossing each other at an oblique angle. The rotational angle is derived mathematically from the tangential contact between yarns. Compatible voxelised mesh and

¹ Open source software http://texgen.sourceforge.net/index.php/Main_Page

periodic boundary conditions for the sheared domain have also been implemented. The CTE predictions from the unit cell analysis are then validated against experimental data.

GEOMETRIC DESCRIPTION OF FABRIC SHEAR

For shear well below the locking angle, the changes in a fabric are predominantly due to geometric constraints, causing (1) re-orientation of tow path; (2) rotation of tow cross-section; (3) slight change of cross-section shape. These changes can be approximated by a geometric approach, without resorting to an expensive finite element model. A simplistic approach is described here to represent fabric shear based on the following principles and assumptions (P&A):

- (i) Total volume of yarns, as well as overall fibre volume fraction, is constant for fabric subjected to shear smaller than the locking angle;
- (ii) Either warp or weft yarn path is re-oriented by a shear angle β ;
- (iii) Rotation of yarn cross-section is due to tangential contact of two yarns;
- (iv) Change of yarn cross-section shape is such that yarn intersections are avoided and total volume is conserved.

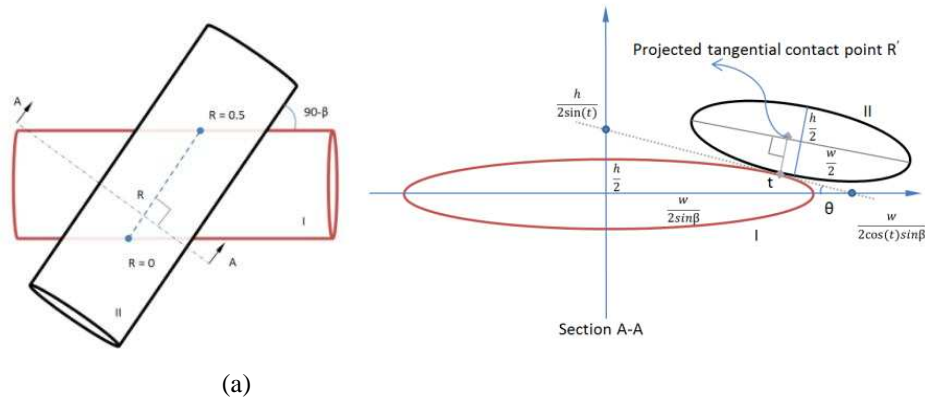


Figure 1. (a) Two identical elliptical cylinders I & II crossing over each other; (b) Surface tangent between two ellipses at Sectional view A-A of (a).

Figure 1 (a) idealises two initially perpendicular yarns subjected to a shear angle β . According to P&A (ii), Yarn II is re-orientated at an angle $(90-\beta)$ to Yarn I.

Based on P&A (iii) for rotational angle of the yarn cross-section, a mathematical expression is obtained to relate yarn cross-sectional width (w), yarn cross-sectional height (h), shear angle (β) and contact point (at normalised length, R). For any contact point at distance R between Yarn I and II (where R is a normalised length, $0 < R < 0.5$, Figure 1(a)), a sectional view A-A in Figure 1(b) illustrates the tangential relationship of two elliptical cross-sections to determine the rotational angle θ . The parametric equations of Ellipse I are

$$\begin{aligned}
 x &= \frac{w}{2\sin\beta} \cos t \\
 y &= \frac{h}{2} \sin t \quad Eq(1)
 \end{aligned}$$

The eccentricity parameter t in Eq(1) can be expressed in terms of the contact point at distance R along the axis of yarn II :

$$\cos t = 1 - 4R \quad Eq(2)$$

The tangential angle would be around 90 degrees at the contact regions near $R = 0$ and $R = 0.5$. This would introduce an unrealistic rotation of the yarn cross-section, hence the projected tangential contact point R' is taken at a distance from the contact point R. After testing on a range of textiles, the distance at $1/10^{\text{th}}$ of the yarn width w from R was found to give good

results across the range and this is the value which has been used in the implementation in TexGen.

This gives:

$$R' = R + \frac{\frac{w}{10} \sin \beta}{2w} = R + \frac{1}{20} \sin \beta \quad \text{when } 0 \leq R \leq 0.25$$

$$R' = R - \frac{\frac{w}{10} \sin \beta}{2w} = R - \frac{1}{20} \sin \beta \quad \text{when } 0.25 \leq R \leq 0.5$$

Substitute R' in Eq (2),

$$\cos t = \begin{cases} 1 - 4R - \frac{1}{5} \sin \beta & \text{when } 0 \leq R \leq 0.25 \\ 1 - 4R + \frac{1}{5} \sin \beta & \text{when } 0.25 \leq R \leq 0.5 \end{cases} \quad \text{Eq(3)}$$

The tangential angle θ is calculated based on the intersection point with axes X and Y, shown in Figure 1 (b),

$$\sin \theta = \frac{\tan \theta}{\sqrt{1 + \tan^2 \theta}} = \pm \frac{1}{\sqrt{1 + \left(\frac{w}{h \sin \beta}\right)^2 \tan^2 t}} = \pm \frac{1}{\sqrt{1 + \left(\frac{w}{h \sin \beta}\right)^2 \left(\frac{1}{\cos^2 t} - 1\right)}} \quad \text{Eq(4)}$$

By substituting $\cos(t)$ from Eq (3) into Equation (4), the rotational angle can be determined at any contact point along the yarn path.

AUTOMATION IN TEXGEN

In order to simplify and automate geometric modelling of sheared textiles, an extension to the automated “2D wizard” has been implemented in TexGen, allowing a shear angle to be specified and enabling an option to create a sheared domain. After specification of the weave pattern, the textile is automatically generated. Nodes are created on the yarn paths at each crossover point between warp and weft yarns; spacings are adjusted according to the shear angle giving an idealised geometry with all yarns having constant, elliptical cross-sections.

Specification of a sheared textile without further modification results in a large number of intersections. A “refine” option has been implemented in order to remove intersections and to create a more realistic textile model. First, the section interpolation is set to allow multiple cross-sections along the yarn length, thereby allowing changes in cross-section along the yarn.

Four extra cross-sections are inserted, giving five equispaced sections with values of R , as specified in the previous section, from 0.005 to 0.495 (including the section at the node where $R=0.25$). The rotation at each of these sections is shown in Figure 2(a) and can be seen in Figure 2(b) where two of the yarns have been removed for clarity.

Based on P&A (iv), changes are made to the yarn cross-section shape to minimise any remaining interference between yarns. A function within the 2D wizard finds intersections between sections and the surface meshes of adjacent yarns and adjusts points on the section, replacing the original elliptical section with a polygonal section.

It has been observed that in real textiles the surface yarns tend to flatten and that there is an offset between the centre of one yarn and the point at which the surface yarn passing over it drops away, shown in Figure 3(a). In the automatically generated, unrefined, TexGen model the surface tow would drop away immediately from the node over the centre of the yarn, following the contour of the yarn it crosses. Also, where interference has been corrected there will have been loss of volume in the yarns which would result in decreased volume fraction of the textile.

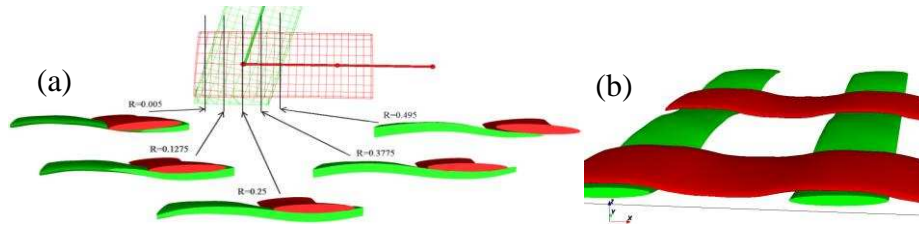


Figure 2. (a) Yarn rotations for different values of R; (b) Rotated yarns in plain weave textile

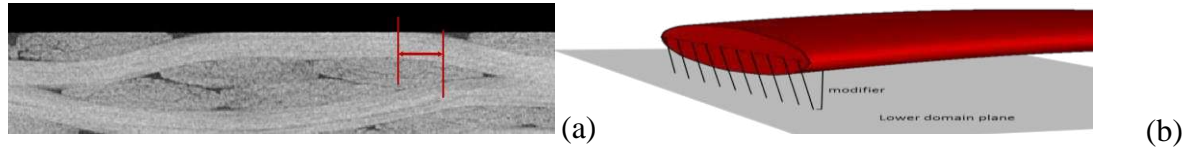


Figure 3. (a) Tow drop offset; (b) Intersection of section points with bottom domain plane

In order to address both of these issues an algorithm has been developed which allows the yarn to be adapted at each cross-section. It is assumed that each yarn is constrained to lie within the fabric thickness specified in the wizard. For each section a set of modifiers are calculated based on the intersection between a line perpendicular to the centreline of the polygon, passing through one of the points on the perimeter, and either the upper or lower plane parallel to the z axis and specified by the thickness. This is shown in Figure 3(b). Modifiers of less than unity are applied immediately, thus constraining the yarn to the specified fabric thickness. An iterative method is then used to extend the points on the polygon along the line of each modifier, using the original yarn area and maximum extension given by the intersection with the plane as constraints.

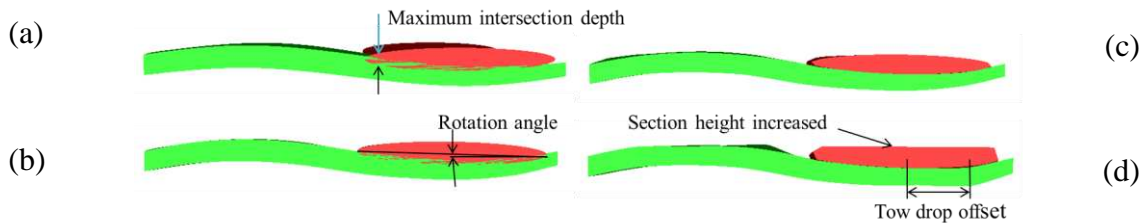


Figure 4. Refinement stages, (a) Unrefined; (b) Rotation only; (c) Rotation and intersection correction; (d) Rotation, intersection correction and adjusted section height.

Figure 4 shows a pair of crossing yarns at different stages of the build textile process. Figure 4(a) shows the yarns before refinement. After rotation, Figure 4(b), the size of the maximum intersection is reduced and the intersections are more evenly distributed. Intersection correction removes these intersections, Figure 4(c), but results in loss of volume from the yarn. The final stage of the refinement increases the height of the upper yarn, in this case to the limit specified by the overall fabric thickness. The side view of the lower yarn shows the tow drop offset produced by the height adjustment at different sections along the yarn.

THERMAL MECHANICAL ANALYSIS

For periodicity it is necessary to apply translational symmetry to formulate the boundary conditions. Positioning the unit cell at a shear angle β , as in Figure 5, the periodic formulation was derived from a generic form [9].

Corresponding nodes on Faces A & B can be mapped onto each other and their relative displacements are:

$$\begin{aligned} -u|_B + u|_A - S_2 \varepsilon_x^0 &= 0 \\ -v|_B + v|_A &= 0 \\ -w|_B + w|_A &= 0 \end{aligned} \quad Eq(5)$$

Faces C and D:

$$\begin{aligned} -u|_D + u|_C - S_1(\varepsilon_x^0 \sin \beta + \gamma_{xy}^0 \cos \beta) &= 0 \\ -v|_D + v|_C - S_1 \varepsilon_y^0 \cos \beta &= 0 \\ -w|_D + w|_C &= 0 \end{aligned} \quad Eq(6)$$

Faces E and F orthogonal to Z (Thickness C):

$$\begin{aligned} -u|_E + u|_F - C\gamma_{xz}^0 &= 0 \\ -v|_E + v|_F - C\gamma_{yz}^0 &= 0 \\ -w|_E + w|_F - C\varepsilon_z^0 &= 0 \end{aligned} \quad Eq(7)$$

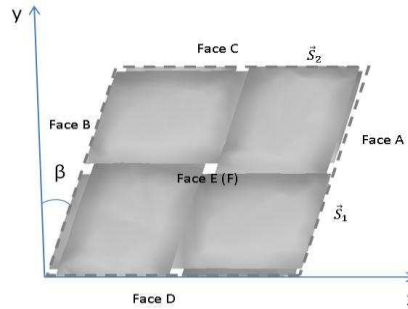


Figure 5. Periodic boundary set-up for a unit cell of sheared woven fabric

In addition, there are a set of similar equations applied to edges and vertices (corner points) of the unit cell to complete the boundary setups.

The thermal mechanical analysis was performed in ABAQUS StandardTM as a static analysis with a temperature perturbation of 1 degree. For composites with sheared fabric reinforcement, it is more convenient to express the coefficients of thermal expansion as a tensor in the local coordinate system. The CTE tensor is recovered from the strain tensor for the unit cell under the temperature perturbation.

MATERIALS AND EXPERIMENTS

Laminates were manufactured from a plain weave dry fabric, Hexcel CF0504 (3K HTA 5131 carbon fibres, 200 gsm, 5 ends per cm) and CYTEC MTM46 resin, using resin film stacking [10]. Three 10-ply laminates with $V_f = 47.5\%$ were made under these conditions: (1) un-sheared, (2) 16° shear and (3) 20° shear. The consolidation used an autoclave at 6 bar, 5 hours initial cure at 80°C , ramp rate $2^\circ\text{C}/\text{min}$. After cooling below 60°C and release of pressure, the laminates were post-cured free standing for 1 hour at 120°C . Shown in Table 1, the geometry was measured from microscopic images of laminate sections.

Table 1 Geometry of single ply fabric CF0504

Yarn width	Yarn height	Yarn in-plane spacing	Laminate thickness
1.76mm	0.16mm	2.03mm	2.4mm

The elastic and thermal properties for HTA fibre were obtained from the literature where direct experimental measurements were made [11-14]. Yarn in the cured laminate was treated as a UD composite with $V_f = 65\%$. Yarn properties were derived from a micro-mechanical finite element model. These data, as listed in Table 2, were used as the input parameters for the FE models of the laminates.

The cured laminates were then cut into small rectangular prisms (5mm x 40mm x 2.4mm, width x length x thickness) along specified directions. The CTE measurements were made

using a pushrod dilatometer, Netzsch DIL 402C. The push-rod dilatometer measured the change along the length dimension, which would be a combination of shear and extension (shrinkage) for highly anisotropic sheared fabric composites.

Table 2 Elastic and thermal properties of the laminate constituents

	Fibre	Resin	Yarn
E_{11} (GPa)	235	2.7	153
E_{22}, E_{33} (GPa)	15		7.86
G_{12}, G_{13} (GPa)	15		3.55
G_{23} (GPa)			2.66
ν_{12}	0.3	0.4	0.33
ν_{23}	0.3		0.48
α_{11} ($^{\circ}\text{C}/\text{K}$)	-0.4	40	-0.12
α_{22} ($^{\circ}\text{C}/\text{K}$)	10		19.7
α_{33} ($^{\circ}\text{C}/\text{K}$)	10		19.7

A correlation is found that the measured change of the sample length in the dilatometer is expressed by the thermal strains

$$\Delta L = L_1 - L_0 = L_0 \varepsilon_x + W_0 |\gamma_{xy}|$$

As a result, the measured CTE is

$$\alpha_{dilatometer} = \frac{\Delta L}{L_0 \Delta T} = \frac{\varepsilon_x}{\Delta T} + \frac{W_0 |\gamma_{xy}|}{L_0 \Delta T} = \alpha_{xx} + \frac{W_0}{L_0} \alpha_{xy} \quad Eq(8)$$

where in the current experiment, $W_0 = 5\text{mm}$, $L_0 = 40\text{mm}$; α_{xx} , α_{xy} are predicted by the unit cell model. This enables a direct correlation of thermal properties between the lab-scale test piece and the material in large composite structures represented by a unit cell model with periodicity.

RESULTS AND DISCUSSION

For the three laminates, non-shear, 16° shear and 20° shear, the unit cells were first generated in the TexGen 2D wizard as single plies, shown in Figure 6 Upper. The importance of finite laminate thickness and random nesting was recognized in the test materials. Hence ten plies of fabric were collated with randomness in both warp and weft directions, sampled by a Latin Hypercube method[15], shown in Figure 6 Lower. The periodicity was removed in the thickness direction for these unit cells, while maintaining the in-plane periodic boundaries.

The finite element analysis was performed in ABAQUS using uniform voxelised elements. The converged mesh size was found, using in total 2 million elements (100x100x200). The CTE predictions are listed together with the experimental data in Table 3. Three randomly nested laminates based on a Latin Hypercube method were modelled for each case, resulting in small standard deviations of 0.5%. Both the experimental and numerical data of CTEs show increasing anisotropy for increasing degrees of shear. A consistently good match within 5% error was found between the predictions from the 10-ply nested laminate unit cell and the

experiments for the laminates with non-shear and 20° shear plies. In the case of the 16° shear laminate, the discrepancy is slightly higher at 12.9%. A plausible explanation of the difference could be due to the error at the manufacturing stage. It was possible that 16° shear angle was not achieved due to fabric relaxation before consolidation. Consequently the measured CTE was lower than the expected value with a fixed shear angle 16°.

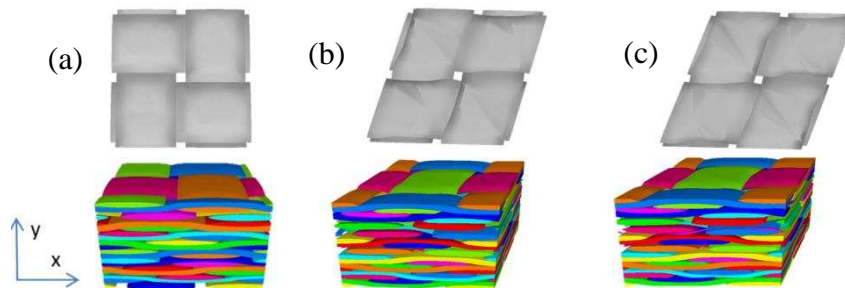


Figure 6. Unit cells representing single ply (upper) and 10-ply laminates (lower) with each ply of (a) non-shear, (b) 16° shear and (c) 20° shear

Table 3. Comparison of predicted CTEs with the experimental data

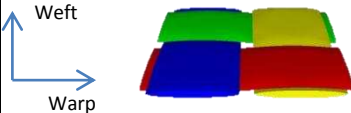
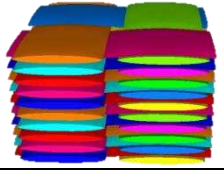
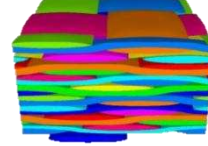
CTE ($\times 10^{-6}$ /K)	Non-shear	16° shear	20° shear	
α_{xx}	2.170	1.422	1.240	
α_{yy}	2.160	4.960	6.420	
α_{xy}	0.0071	12.40	14.240	
Prediction ^{Eq(5)}	2.171 ^{in x}	2.97 ^{in x}	3.02 ^{in x}	8.20 ^{in y}
Experiment	2.12	2.63	2.99	8.46
Error (%)	2.4	12.9	1.0	-3.1

The study also aimed to investigate how construction of the unit cell for composite laminates influenced the prediction of CTEs. Two main factors were identified as laminate thickness and ply nesting. Both factors contribute to the anisotropy of elasticity and CTEs in each ply. Unit cell modelling helped quantify the underlying factors. The construction details of each unit cell are listed in Table 4 together with the CTE predictions. A randomly nested 10-ply unit cell with a thickness 2.4mm matched the test sample closely in terms of geometry. The CTE prediction was closest to the experimental data with 2.4% error. Keeping the 10-ply construction with the same thickness, another unit cell with perfectly zero nesting deviated from the prediction by 18.4%. A unit cell of a single ply with in-plane and through-thickness periodicity describes an extra-thick, perfectly stacked laminate with no nesting. The predicted CTE from this model was 50% higher than the experimental data.

CONCLUSIONS

This study has successfully addressed the issues related to unit cell modelling for CTE prediction of textile composites. Based on some basic principles and assumptions, fabric geometry was refined to simulate shear deformation. This refinement process was automated in TexGen to ensure consistency of geometric modelling. A correlation was established and validated between the anisotropic CTE tensor and the measured data from a small laboratory coupon. The reliability and sensitivity of CTE prediction was assessed by the unit models with controlled geometry variations. Two geometric factors of laminate thickness and nesting were found to be significant for textile reinforced composites.

Table 4. Influence of laminate thickness and nesting on CTE

Model	CTE prediction in warp ($\times 10^{-6} / \text{K}$)	Note
Experiment	2.12	
Infinite size in in-plane and thickness, zero nesting, representing by single layer with periodic boundary condition (pbc)	3.20	
Ten layers, no nesting, pbc in-plane	2.51	
Ten layers, random nesting, pbc in-plane (3 laminate models)	2.17±0.01	

ACKNOWLEDGEMENTS

This work was supported by the Engineering and Physical Sciences Research Council [grant number: EP/IO33513/1], through the EPSRC Centre for Innovative Manufacturing in Composites.

REFERENCES

- Radford, D. and T. Rennick, Separating sources of manufacturing distortion in laminated composites. *Journal of Reinforced Plastics and Composites*, 2000. **19**(8): p. 621-641.
- Bowles, D.E. and S.S. Tompkins, Prediction of Coefficients of Thermal Expansion for Unidirectional Composites. *Journal of Composite Materials*, 1989. **23**(4): p. 370-388.
- Dong, C., Development of a Model for Predicting the Transverse Coefficients of Thermal Expansion of Unidirectional Carbon Fibre Reinforced Composites. *Applied Composite Materials*, 2008. **15**(3): p. 171-182.
- Lu, T. and J. Hutchinson, Thermal conductivity and expansion of cross-ply composites with matrix cracks. *Journal of the Mechanics and Physics of Solids*, 1995. **43**(8): p. 1175-1198.
- Ishikawa, T. and T.-W. Chou, In-plane thermal expansion and thermal bending coefficients of fabric composites. *Journal of Composite Materials*, 1983. **17**(2): p. 92-104.
- Naik, N. and V. Ganesh, Prediction of thermal expansion coefficients of plain weave fabric composites. *Composite Structures*, 1993. **26**(3): p. 139-154.
- Fruehmann, R.K., J.M. Dulieu-Barton, and S. Quinn, On the thermoelastic response of woven composite materials. *The Journal of Strain Analysis for Engineering Design*, 2008. **43**(6): p. 435-450.
- Khoun, L., K. Challagulla, and P. Hubert, Thermo-mechanical properties of 5-harness satin fabric composites. *Journal of Composite Materials*, 2012. **46**(25): p. 3121-3136.
- Li, S., C.V. Singh, and R. Talreja, A representative volume element based on translational symmetries for FE analysis of cracked laminates with two arrays of cracks. *International Journal of Solids and Structures*, 2009. **46**(7-8): p. 1793-1804.
- Smitheman, S. A., Q.P.V.Fontana, M. G. Davies, S. Li, I. A. Jones, A. C. Long and W. Ruijter. Unit cell modelling and experimental measurement of the elastic and thermoelastic properties of sheared textile composites. in *International Conference on Textile Composites TEXCOMP 10*. 2010. Lille, France.
- Hobbiebrunken, T., et al., Influence of non-uniform fiber arrangement on microscopic stress and failure initiation in thermally and transversely loaded CF/epoxy laminated composites. *Composites Science and Technology*, 2008. **68**(15-16): p. 3107-3113.
- Hobbiebrunken, T., et al., Microscopic yielding of CF/epoxy composites and the effect on the formation of thermal residual stresses. *Composites Science and Technology*, 2005. **65**(10): p. 1626-1635.
- Fiedler, B., et al., Finite-element modeling of initial matrix failure in CFRP under static transverse tensile load. *Composites Science and Technology*, 2001. **61**(1): p. 95-105.
- Pradere, C. and C. Sauder, Transverse and longitudinal coefficient of thermal expansion of carbon fibers at high temperatures (300–2500K). *Carbon*, 2008. **46**(14): p. 1874-1884.
- McKay, M.D., R.J. Beckman, and W.J. Conover, Comparison of three methods for selecting values of input variables in the analysis of output from a computer code. *Technometrics*, 1979. **21**(2): p. 239-245.